JACS
JOURNAL OF THE AMERICAN CHEMICAL SOCIETY
pubs.acs.org/JACS
Article

Ion-Selective Assembly of Supertetrahedral Selenido Germanate Clusters for Alkali Metal Ion Capture and Separation

Zhou Wu, Florian Weigend, Dieter Fenske, Tim Naumann, J. Michael Gottfried, and Stefanie Dehnen*

Cite This: J. Am. Chem. Soc. 2023, 145, 3802−3811
Read Online
ACCESS | Metrics & More | Article Recommendations | Supporting Information

ABSTRACT: Supertetrahedral chalcogenido (semi)metalate cluster-based frameworks possess high selectivity for alkali metal cations, matching the specific charge density of their inner surfaces, which enables their use as ion-exchange materials. Aggregates of the supertetrahedral chalcogenido metalate cluster offer even new perspectives for metal ion capture and separation. Herein, we report on ionothermal preparation of two corresponding model compounds, $(C_2C_1Im)_7[Cs@Ge^{II}_4(Ge^{IV}_4Se_{10})_4]$ (**1**) and $(C_2C_1Im)_{10}[Na_5(CN)_6@Cu_6(Ge_4Se_{10})_4(Cu)]$ (**2**). Their formation is reliant on one specific cation type each, Cs^+ for **1** and Na^+ for **2**, thus providing promising separation potential during crystallization. Compound **1** is based on the largest discrete binary selenido germanate cluster reported to date and the first mixed-valent chalcogenido germanate(II/IV) supertetrahedron. Moreover, it adds to the few examples of chalcogenides capable of capturing Cs^+ ions. Its high selectivity for Cs^+ compared to that of Li^+, Na^+, K^+, and Rb^+ was confirmed by single-crystal X-ray diffraction, energy-dispersive X-ray spectroscopy, and electrospray ionization mass spectrometry. Quantum chemical studies indicate that smaller ions, K^+ and Rb^+, could also be embedded in an isolated cluster assembly, but as the cluster aggregate slightly distorts for crystallization, the selectivity for Cs^+ becomes exclusive in the salt. The anionic substructure of compound **2** is based on a two-dimensional network of supramolecular assemblies and exhibits an exclusive preference for Na^+. This work thus provides the first comprehensive insight into the selective incorporation of specific alkali metal ions into supramolecular aggregates of supertetrahedral chalcogenide clusters, as a promising basis for new ion trapping techniques—especially for heavy alkali metal ions that pose environmental challenges.

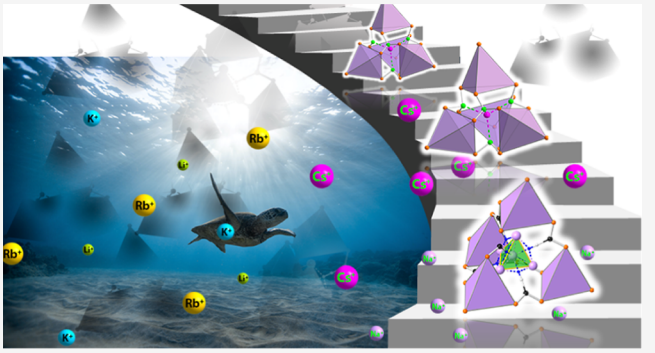

1. INTRODUCTION

The removal of Cs^+ ions and the recovery of other alkali metal ions (especially Li^+, Na^+, and K^+) from wastewater are essential steps for solving the environmental crisis and achieving energy conversion. These issues have therefore been of increased significance and simultaneously an advancing research topic during the past years.[1−3]

Due to the similar chemical properties, alkali metal cations often coexist in nature. It is thus not only strongly desired but also challenging to develop efficient methods to improve separation techniques possessing high ion selectivity. As a result, a variety of methods, including ion-exchange,[4,5] liquid−liquid extraction,[6,7] solid−liquid extraction,[8,9] and film separation,[10,11] have been proposed to further improve the separation efficiency (Scheme 1). In spite of only small differences in the ionic radii and charge densities of Na^+, K^+, and Ca^{2+}, an artificial Na^+-selective ionic device based on crown-ether crystals was developed, for instance, which achieves a high selectivity of Na^+ toward K^+ and Ca^{2+}.[12] In addition, crystalline silicotitanate showed both high capacity and selectivity for Cs^+ during the ion-exchange process, even in solutions comprising NaOH concentrations of 1−7 mol/L,[13] and also, zeolite-type chalcogenides showed promising uptake rates for heavy ions.[14,15] According to these findings, the slight yet notable differences in the ionic radii r_+ of the alkali metal ions (A^+) play the most important role in increasing the separation efficiency. Therefore, the performance of such materials can be amplified by selective crystallization owing to the lattice energy's general dependency from the cation's charge Z^+ and the ionic radius as Z^+/r_+.

Compounds comprising supertetrahedral chalcogenido metalate clusters have been extensively studied from synthesis aspects to the application perspective and in particular for applications in selective removal of radionuclide or heavy metal elements.[16,17] Corresponding salts show high selectivity for capturing relatively "soft" cations Cs^+ and Sr^{2+} as compared to

Received: December 19, 2022
Published: January 31, 2023

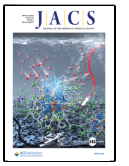

Scheme 1. Summary of Reported Alkali Metal Ion Separation Approaches: (a) Solid−Liquid Ion-Exchange, (b) Ion Separation by Liquid−Liquid Extraction, (c) Ion Separation in Films, and (d) Ion-Selective Cluster Assembly (Presented Herein)

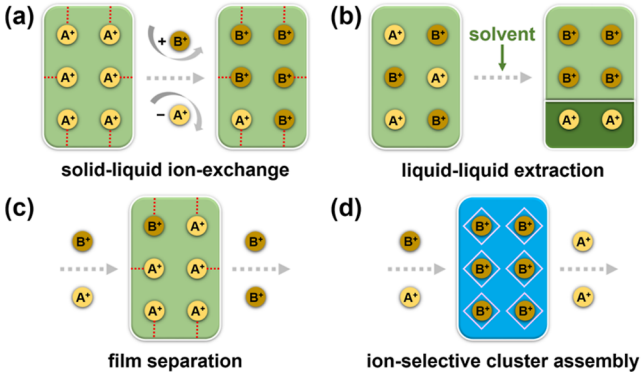

the "harder" alkali or alkaline earth ions, which is attributed to the stronger interaction of the former with the "soft" inner chalcogenide surface of such frameworks.[15,18,19] However, none of these pioneering reports focused on selective crystallization of such compounds for the separation of alkali metal cations.

Given the recent progress in chalcogenide cluster chemistry,[20−29] we consider supertetrahedral chalcogenido metalate cluster compounds (or networks of such clusters) with suitable cavities to be excellent candidates for the selective incorporation of A^+ ions. However, most compounds based on supertetrahedral chalcogenido metalate clusters that have been reported so far are structurally templated by organic ammonium cations (from neutral amines or ionic liquid cations), which occupy the cavities and can hardly be replaced. In contrast, much fewer compounds have been known in which the clusters co-crystallized with A^+ counterions. We have therefore searched for a method that allows a combination of both, thus enabling A^+-selective crystallization, on which we report herein (Scheme 1).

In this work, we demonstrate the ion-selective cluster assembly as a new approach, using the example of two novel compounds. Both are based on the supramolecular assembly of supertetrahedral selenido germanate clusters to form pseudo-P2-type and pseudo-T2,2-type superclusters. The first one, $(C_2C_1Im)_7[Cs@Ge^{II}_4(Ge^{IV}_4Se_{10})_4]$ (**1**), comprises a mixed-valent anionic substructure that represents both the largest selenido germanate cluster reported to date and the first mixed-valent supertetrahedral chalcogenido germanate (+II/+IV) compound. The second compound, $(C_2C_1Im)_{10}[Na_5(CN)_6@Cu_6(Ge_4Se_{10})_4(Cu)]$ (**2**), is based on a framework of related, yet heterometallic supercluster anions. The title compounds were obtained by joint templating effects of A^+ (= Cs^+ in **1** and Na^+ in **2**) and ionic liquid cations $(C_2C_1Im)^+$ (= 1-ethyl-3-methyl-imidazolium). We demonstrate that the salts possess high selectivity for either heavy (**1**) or light (**2**) types of A^+ cations and as such show very promising in situ separation characteristics. The exclusive crystallization with either Cs^+ or Na^+ was proven by corresponding cross-experiments in combination with thorough analyses by means of single-crystal X-ray diffraction (SC-XRD), energy-dispersive X-ray (EDX) spectroscopy, and electrospray ionization mass spectrometry (ESI-MS), taking advantage of the good solubility of compound **1** in dimethylformamide (DMF). Moreover, comprehensive density functional theory (DFT) calculations on the (hypothetic) series of clusters with Li^+, Na^+, K^+, Rb^+, or Cs^+ on the central position of the anion in compound **1** indicate that an isolated cluster would also allow for the inclusion of Rb^+ or even K^+, which does not occur, however, when crystallizing the compound. This confirms that the clear preferences of the supercluster architectures for the incorporation of said alkali metal Cs^+ ions in compound **1** are closely connected to the crystalline state.

2. EXPERIMENTAL SECTION

2.1. Syntheses. General: All synthetic steps were performed under an argon atmosphere using standard Schlenk or glovebox techniques. $[Cs_4(H_2O)][Ge_4Se_{10}]$,[30] $[Na_4(H_2O)_{14}][GeSe_4]$,[31] $[Li_4(H_2O)_{20.33}]$-$[Ge_4Se_{10}]$,[32] $Na_4[Ge_4Se_{10}]$,[33] $[K_4(H_2O)_3]$-$[Ge_4Se_{10}]$,[34] $Rb_4[Ge_4Se_{10}]$,[35] and $[K_4(H_2O)_4][GeSe_4]$[36] were synthesized according to literature procedures. 2,6-Dimethylmorpholine (DMMP; Sigma-Aldrich, 99.8%) was dried over P_2O_5, distilled, and stored over a molecular sieve (3 Å). 1-Ethyl-3-methyl-imidazolium tetracyanoborate, $(C_2C_1Im)[B(CN)_4]$ (Sigma-Aldrich, 99.5%), copper cyanide, CuCN (Riedel-de-Haen, 99%), and copper acetate monohydrate, $Cu(OAc)_2{\cdot}H_2O$ (Fluka Chemika, 99%) were degassed before use. The general synthesis procedures of compound **1** and polymorphs **2a** and **2b** are summarized in Scheme 2 and outlined in detail below.

Synthesis of $(C_2C_1Im)_7[Cs@Ge^{II}_4(Ge^{IV}_4Se_{10})_4]$ (**1**): 40 mg of $[Cs_4(H_2O)][Ge_4Se_{10}]$ (0.025 mmol), 500 μL of $(C_2C_1Im)[B(CN_4)]$ (2.300 mmol), and 50 μL of DMMP (0.406 mmol) were combined in a borosilicate glass ampoule, which was sealed air-tight thereupon. The ampoule was heated to 150 °C at a heating rate of 30 °C/h, kept at 150 °C for 72 h, and then cooled down to room temperature at a cooling rate of 5 °C/h. Yellow, block-shaped crystals of **1** (Figure S1a) were obtained in ∼72.9% yield (20.1 mg) with respect to $[Cs_4(H_2O)][Ge_4Se_{10}]$.

Synthesis of $(C_2C_1Im)_{10}[Na_5(CN)_6@Cu_6(Ge_4Se_{10})_4(Cu)]$ (**2**): 40 mg of $[Na_4(H_2O)_{14}][GeSe_4]$ (0.055 mmol), 8 mg of CuCN (0.089 mmol; for polymorph **2a**) or 10 mg of $Cu(OAc)_2{\cdot}H_2O$ (0.050 mmol;

Scheme 2. Summary of the Reactions Yielding Compounds 1, 2a, and 2b[a]

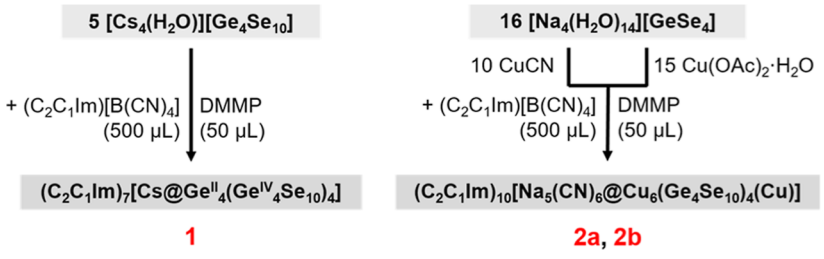

[a]All reactions were carried out at 150 °C for 3 days. Soluble/volatile byproducts and Cu_2Se are not shown for clarity.

https://doi.org/10.1021/jacs.2c13523
J. Am. Chem. Soc. 2023, 145, 3802−3811

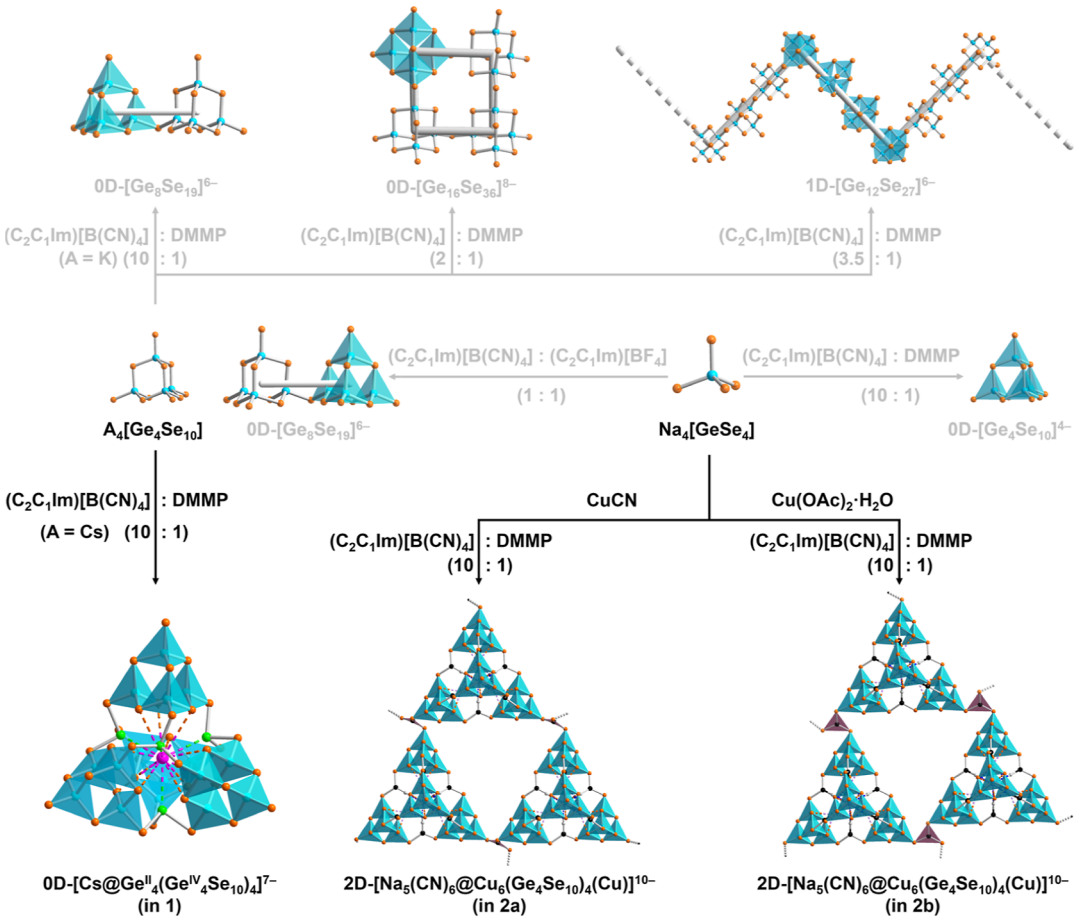

Figure 1. Application of salts of $[GeSe_4]^{4-}$ or $[Ge_4Se_{10}]^{4-}$ anions for the ionothermal synthesis in $(C_2C_1Im)[B(CN)_4]$:DMMP of complex anionic substructures based on supertetrahedral $[Ge_4Se_{10}]^{4-}$ units in known compounds (center and top, gray arrows and formulas) and in new compounds **1**, **2a**, and **2b** reported in this work (bottom, black arrows and formulas; all reactions were performed at 150 °C for 3 days). Relative amounts of $(C_2C_1Im)[B(CN)_4]$ and DMMP are given as v/v ratios. For more details, see the Experimental Section. Crystallographically indistinguishable Ge, Cu, and Se atoms were assigned based on their characteristic coordination modes; compositions were verified by means of EDX measurement. Atom color code: Ge^{IV}—turquoise, Ge^{II}—green, Se—orange, Cs—pink; N—blue, C—gray, Na—lilac, and Cu—black.

for polymorph **2b**), 500 μL of $(C_2C_1Im)[B(CN_4)]$ (2.300 mmol), and 50 μL of DMMP (0.406 mmol) were combined in a borosilicate glass ampoule, which was sealed air-tight thereupon. The ampoule was heated to 150 °C at a heating rate of 30 °C/h, kept at 150 °C for 72 h, and then cooled down to room temperature at a cooling rate of 5 °C/h. A few red plate-like crystals of **2a** or **2b**, respectively (Figure S1b,c), were obtained.

2.2. Single-Crystal X-ray Diffraction. Single-crystal diffraction data were collected on an area detector system Stoe StadiVari (**1**; T = 150 K, Ga-Kα radiation, λ = 1.34143 Å) or on a Bruker D8Quest with a CMOS detector (**2a**, **2b**; T = 100 K, Mo-Kα radiation, λ = 1.54186 Å). The structures were solved by dual-space methods implemented in SHELXT from SHELXL-2018/136[37] and refined by full matrix least-squares methods against F^2 using the SHELXL program.[38] Measurement, structure solution, and refinement results, as well as details on the back Fourier transform procedure using the SQUEEZE algorithm in the PLATON program package,[39,40] are detailed in Tables S1–S3. Figures were created using Diamond 4.5.[41] Crystallographic data for the structures reported in this paper have been deposited with the Cambridge Crystallographic Data Center: CCDC-2178545 (**1**), CCDC-2178546 (**2a**), and CCDC-2178547 (**2b**). Copies of the data can be obtained free of charge on application to CCDC (Email: deposit@ccdc.cam.ac.uk).

2.3. Energy-Dispersive X-ray Spectroscopy. EDX analyses of single crystals (Figures S12–S14, S16, and S23) were carried out using an EDX device Voyager 4.0 of Noran Instruments coupled with an electron microscope CamScan CS 4DV. Data acquisition was performed with an acceleration voltage of 15 kV and an accumulation time of 100 s.

2.4. X-ray Photoelectron Spectroscopy. X-ray photoelectron spectroscopy (XPS) was carried out on a SPECS Phoibos 150 electron energy analyzer, using monochromatized Al Kα radiation operated at 30 eV pass energy. The spectrum (Figure S5) was recorded in ultrahigh vacuum after cleaning the surface by sputtering with Ar^+ ions. The measurement was performed with low photon flux to avoid charging effects and beam damage.

2.5. Electrospray Ionization Mass Spectrometry. ESI mass spectra were recorded using a Thermo Fisher Scientific Finnigan LTQ-FT spectrometer in a negative ion mode. Single crystals of the compounds were dissolved in freshly distilled DMF. The solutions were injected into the spectrometer with gas-tight 250 μL Hamilton syringes by syringe pump infusion. The spectra are displayed in Figures S17–S21, and selected spectra are provided in Figure 5.

2.6. Quantum Chemical Calculations. The calculations[42] were performed at the DFT(PBE[43]) level. The quasi-relativistic all-electron approach DLU-X2C[44,45] in its scalar-relativistic variant was applied with optimized triple-zeta basis sets.[46] The conductor-like screening model (COSMO)[47] was used for charge compensation with default parameters throughout. All structures were fully optimized without symmetry restrictions.

3. RESULTS AND DISCUSSION

3.1. Syntheses and Crystal Structures. The three title compounds were obtained from ionothermal reactions in the

https://doi.org/10.1021/jacs.2c13523
J. Am. Chem. Soc. 2023, 145, 3802–3811

ionic liquid $(C_2C_1Im)[B(CN_4)]$ in the presence of DMMP at 150 °C for 3 days. As shown in Scheme 2, crystals of compound **1** were obtained upon treating $[Cs_4(H_2O)][Ge_4Se_{10}]$ in a 10:1 (v/v) mixture of $(C_2C_1Im)[B(CN_4)]$ and DMMP. Red plate-like single crystals of compounds **2a** and **2b** were prepared under the same reaction conditions by using other starting materials. For preparing **2a**, $[Na_4(H_2O)_{14}][GeSe_4]$ was reacted with CuCN. To explore whether the $(CN)^-$ anions in the structure of **2a** originated from the copper salt alone or also from the complex ionic liquid anion, $[B(CN)_4]^-$, an alternative approach was tested employing $Cu(OAc)_2{\cdot}H_2O$. This treatment afforded the same compound, as polymorph **2b**, yet in lower yields than that obtained for **2a**. An overview of the comprehensive investigations is provided in Figure 1, and the crystal structures of the new compounds are discussed below.

It is worth noting that the use of $[Cs_4(H_2O)][Ge_4Se_{10}]$ or $[Na_4(H_2O)_{14}][GeSe_4]$ is essential for successfully synthesizing the title compounds **1** and **2**; the compounds were not obtained upon replacement of these salts with $[Li_4(H_2O)_{20.33}][Ge_4Se_{10}]$, $Na_4[Ge_4Se_{10}]$, $[K_4(H_2O)_3][Ge_4Se_{10}]$, $Rb_4[Ge_4Se_{10}]$, or $[K_4(H_2O)_4][GeSe_4]$ as single-source reactants, unless additional CsCl or NaCl was added to the respective reactions. With these investigations, we expand on recent studies of the use of $[Ge_xSe_y]^{4-}$ anions in $(C_2C_1Im)[B(CN_4)]$ by exploring the effect of varied counterions on (a) their templating role and (b) the selectivity of the anionic substructures for the cations' incorporation in the finite cluster and the cluster network architectures.

Compound **1** crystallizes in the orthorhombic crystal system, space group $P2_12_12_1$ with four formula units per unit cell [12307.8(8) Å^3; Figure 2a; more details to be found in the Supporting Information]. The crystallographically indistinguishable Ge and Se atoms were assigned according to their characteristic coordination modes; their relative amount was verified by means of EDX analyses (see Supporting Information, Figure S12 and Table S10) and ESI-MS (see below).

As shown in Figure 2b,c, four T2-type $[Ge_4Se_{10}]^{4-}$ anions are connected by four Ge atoms. Corresponding to their pyramidal coordination (Figure S3), those four atoms represent (formal) Ge^{II} sites with a lone pair pointing toward the center of the supramolecular assembly. Compound **1** exhibits a structure related to supertetrahedral P2-type clusters like $[Cu_6Tr_{12}Sn_8S_{44}]^{14-}$ (Tr = Ga and In),[25,48] $[Li_4In_{22}S_{44}]^{14-}$,[49] or $[Cu_{11}In_{15}Se_{16}(SePh)_{24}(PPh_3)_4]$[50] (Tn represents a supertetrahedral cluster with n layers of connected tetrahedra/metal atoms; Pn represents a pentasupertetrahedral cluster, constructed by adding four supertetrahedral Tn clusters onto the four faces of a supertetrahedral Tn cluster with an inverse metal/chalcogen composition). However, in contrast to the pristine P2-type architecture (see Figure 2d), the inner moiety is not an anti-T2-supertetrahedron but consists of a central Cs^+ cation and the four Ge^{II} atoms. This defect- or pseudo-P2-type architecture was only described for a related Sn^{II}/Ge^{IV} compound so far, $(C_4C_1C_1im)_7[Cs@Sn^{II}_4(Ge^{IV}_4Se_{10})_4]$ [with $(C_4C_1C_1Im)^+$ representing 1-butyl-2,3-dimethylimidazolium cations].

With a total of 20 Ge and 40 Se atoms, the anion in **1** is the largest selenido germanate cluster architecture reported to date. The co-existence of both Ge^{IV} and Ge^{II} was unambiguously confirmed by high-resolution XPS of **1** (Figure S5), and the different valence states of the respective atomic

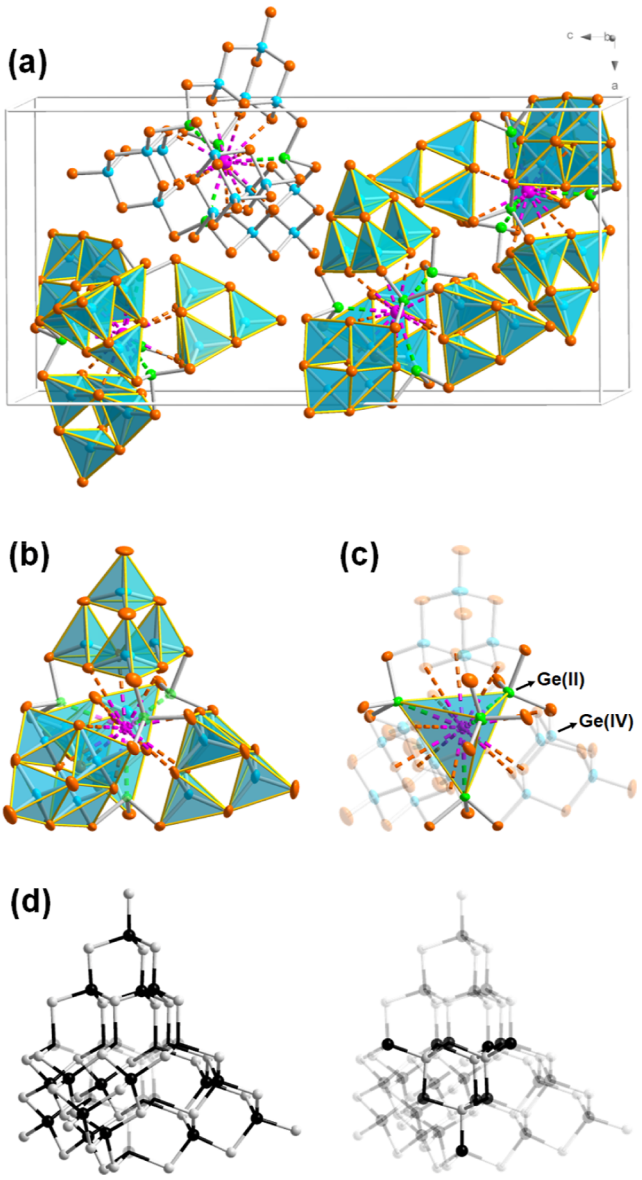

Figure 2. (a) View of the (extended) unit cell of compound **1**. (b) Molecular structure of the $[Cs@Ge^{II}_4(Ge^{IV}_4Se_{10})_4]^{7-}$ anion in compound **1** in the crystal; atoms are shown as thermal ellipsoids at the 50% probability level (color code: Ge^{IV}—turquoise, Ge^{II}—green, Se—orange, and Cs—pink); crystallographically indistinguishable Ge and Se atoms were assigned based on their characteristic coordination modes; the asymmetric unit with the atom labeling scheme is given in Figure S2. (c) Highlight of the inner moiety comprising the Cs^+ ion, 4 Ge^{II} sites, and 12 Se atoms coordinating the latter; the connection of the Cs^+ ion to 12 other Se atoms is illustrated by dashed lines. (d) Structure of the P2 supertetrahedral cluster in $[Cu_6Tr_{12}Sn_8S_{44}]^{14-}$ (Tr = Ga and In) for comparison,[48] emphasizing the four outer T2 units (left) and the inner anti-T2 unit (right), respectively.

positions were additionally rationalized by BVS calculations (Tables S5−S8). A comparison of the observed Ge^{II}−Se and Ge^{IV}−Se bond lengths with those of related compounds (Table S9) led to the same conclusion. Hence, the cluster also represents a rare example of an inorganic mixed-valent Ge(II/IV) compound—and the first one observed in supertetrahedral chalcogenide germanate cluster chemistry to date.

https://doi.org/10.1021/jacs.2c13523
J. Am. Chem. Soc. 2023, 145, 3802−3811

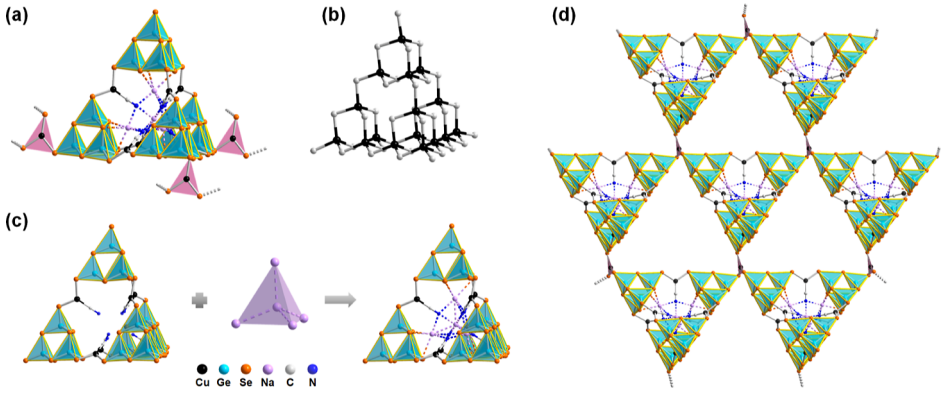

Figure 3. (a) Molecular structure of one pseudo-T2,2-like $[Na_5(CN)_6@Cu_6(Ge_4Se_{10})_4(Cu)]^{10-}$ supercluster in compound **2a** (as an example for compounds **2a** and **2b**) along with the three $\{CuSe_3\}$ units connecting the supercluster with its neighbors; atoms are shown as thermal ellipsoids at the 50% probability level; crystallographically indistinguishable Cu, Ge, and Se atoms were assigned based on their characteristic coordination modes; the asymmetric units with atom labeling scheme of **2a** and **2b** are displayed in Figures S6 and S7. (b) Structure of the T2,2 defect-supertetrahedral cluster in UCR-22 for comparison.[51] (c) Illustration of the architecture of the supercluster without (left) and with the inner $\{Na_5\}$ moiety for clarity. (d) Fragment of the two-dimensional layer in compound **2a** (imidazolium counterions omitted for clarity). For more details, see the Supporting Information.

Like the related Sn/Ge cluster, the $[Ge^{II}_4(Ge^{IV}_4Se_{10})_4]^{8-}$ cage embeds a Cs^+ ion, which not only plays a significant structure-directing and structure-stabilizing role but also reduces the negative charges of the supercluster from 8− to 7−. The Cs^+ ion is embedded in an inner cavity and stabilized by the lone pairs of the 4 Ge^{II} atoms [Cs···Ge 3.82081(1)−3.8554(1) Å] and 12 Se^{2-} anions [Cs···Se 4.1145(1)−4.3489(1) Å], see Figures 2b,c.

In contrast to the synthesis of $(C_4C_1C_1Im)_7[Cs@Sn^{II}_4(Ge^{IV}_4Se_{10})_4]$ by the ionothermal reaction of $[Cs_4(H_2O)][Ge_4Se_{10}]$, $SnCl_4$, and $[Pt@Bi_{10}][AlBr_4]_4$, compound **1** was synthesized from a single-source precursor, $[Cs_4(H_2O)][Ge_4Se_{10}]$. So far, the in situ reduction of Ge^{IV} to Ge^{II} could not be fully clarified as the reductive power of either selenide or cyanide (or both) would be suitable for it. However, the use of $(C_2C_1Im)[B(CN_4)]$ is mandatory for obtaining the mixed-valent product. We ascribe this to the fact that $(CN)^-$, which is released from the anion, is oxidized to cyanogen, C_2N_2, which under the basic conditions (H_2O plus amine) disproportionates into cyanide and cyanate. In addition, the size of the ionic liquid cation seems to subtly affect the crystallization since we were not able to isolate a compound comprising this cluster anion from $(C_4C_1C_1Im)[BF_4]$—which in turn allowed the crystallization of the Sn/Ge/Se analogue. Apparently, the overall smaller size of the purely Ge-/Se-based anion (edge length Se···Se 15.78−16.01 Å) fits better to the smaller-size $(C_2C_1Im)^+$ cations, while the larger Sn/Ge/Se anion (edge length Se···Se 16.18 Å) is well accommodated within a $(C_4C_1C_1)^+$ counterion environment. Consequently, the packing schemes of the clusters in the crystals of the two compounds differ (Figure S4).

As a consequence of the significant disorder of the organic cations, only some of their C and N atoms could be localized from the difference Fourier map. The corresponding electron density was distracted from the data by means of the back Fourier transform method, implemented as the SQUEEZE algorithm in PLATON.[39,40]

Compounds **2a** and **2b** crystallize in the triclinic crystal system, space group $P\bar{1}$, with unit cell volumes of 7842.1(6) $Å^3$ (**2a**) and 7822.6(5) $Å^3$ (**2b**), respectively (Figures S6 and S7). As compounds **2a** and **2b** differ in structural details only, we will discuss their general structural features together here (details to be found in the Supporting Information). The crystal structure of compound **2a** is displayed in Figure 3, as an example of both **2a** and **2b**.

Similar to the architecture of the anion in compound **1**, four T2-type $[Ge_4Se_{10}]^{4-}$ units are connected in compound **2** to form a supercluster assembly (Figure 3a). However, the way of connection is significantly different in several regards. In this case, not four Ge^{II} atoms, but six Cu^I atoms serve to connect the $[Ge_4Se_{10}]^{4-}$ moieties, which are thus arranged in a different way relative to each other: they are connected along the six edges of a T2,2-related architecture (see Figure 3b; Tp,q-like clusters possess defect Tn-type structures, e.g., the T2,2-type is a defect T4-type architecture lacking a central T2-type cluster connecting four T2-type units) and not *via* the four faces of a P2-related one. Nevertheless, while the T2 units are linked *via* a single μ-bridging atom in a real T2,2-type cluster, the T2 moieties in the pseudo-T2,2 structure of the heterometallic cluster in **2** are connected *via* Se−Cu^I−Se bridges. The anion of **2** therefore represents the first superclusters with such triatomic bridges including transition metal atoms. The edge lengths of the superclusters are larger than they would be in a (hypothetical) Ge/Se-based T2,2 cluster (Figure S8), being 18.3509(5)−18.7436(6) Å in compound **2a** and 18.4181(8)−18.7532(7) Å in compound **2b** (the edges of the Ge-/S-based T2,2 cluster in UCR-22 are 14.27−14.43 Å[51]).

The Cu^I atoms involved in the bridges between the $[Ge_4Se_{10}]^{4-}$ units at the same time belong to an inner unit filling the cavity in these clusters: Besides the two Se^{2-} neighbors from two adjacent T2 clusters, the copper atoms are coordinated by a cyanide group, the presence of which has also been unprecedented in supertetrahedral chalcogenide cluster chemistry. The $(CN)^-$ anions serve as ambident ligands, coordinating to Na^+ atoms with their second donor site. Specifically, the six cyanide ligands bridge the six edges of an inner Na_4 tetrahedron, which is centered by the fifth Na^+ ion that is also coordinated by the six $(CN)^-$ anions, each of which thus acts as an $\eta^1{:}\eta^3$-μ ligand (Figure 3c). The five Na^+ ions, in turn, serve to balance a part of the overall negative charges of the anion but at the same time provide us an opportunity to investigate the selectivity of the cluster

https://doi.org/10.1021/jacs.2c13523
J. Am. Chem. Soc. 2023, 145, 3802−3811

formation toward Na^+ as the stabilizing alkali metal ion and on a long term also the potential Na^+ storage properties of such compounds.

As illustrated in Figures 3d and S9, heterometallic superclusters coordinate to triconnected Cu^I atoms with three of their four terminal Se atoms; this way, they are further assembled into a 2D honeycomb (*hcb*) superlattice, with an overall composition of 2D-{$[Na_5(CN)_6@Cu_6(Ge_4Se_{10})_4(Cu)]^{10-}$}. The slight structural differences between compounds **2a** and **2b** are caused by different relative orientations of the {$Cu(\mu\text{-}Se)_3$} groups that connect the pseudo-T2,2 clusters (see Figure S11a,b; for further details of the slightly differing structures of **2a** and **2b**, see Figures S11c,d).

During structure refinement of **2a**, all ionic liquid cations could be localized from the difference Fourier map. In the case of **2b,** 8 of the 10 counterions were localized and refined explicitly, while the electron density of the two remaining ones needed to be detracted from the data using the back Fourier transform algorithm.

For reactions in supercritical solvents or ionic liquids, the most important templates are commonly ammonium cations or auxiliary amines applied in the reactions. Less attention has been spent on the alkali metal cations that were usually only part of the reactants. Our findings show, however, that they do play a major role for certain compounds, which may be used for the targeted capture or separation of the alkali metal cations. We were thus interested to explore the selectivity of the two compounds for the alkali metal cations stabilizing them in more detail, which was achieved by means of quantum chemical calculations using DFT methods as well as by corresponding cross-experiments followed by SC-XRD, EDX, and ESI-MS studies.

3.2. Quantum Chemical Studies, Exchange Reactions, and Mass Spectrometry. For the identification of metal types being preferred for the encapsulation, DFT calculations addressed the incorporation of A^+ into the discrete cluster assembly of compound **1** by a hypothetical reaction given as eq 1:

$$[Ge_4(Ge_4Se_{10})_4]^{8-} + A^+ \rightarrow [A@Ge_4(Ge_4Se_{10})_4]^{7-} \quad (1)$$

This reaction scheme models the uptake of an alkali metal cation in an empty supercluster (see Figure 4 for A = Cs as an example), thus delivering the binding energies of A^+ to the empty (hypothetical) $[Ge_4(Ge_4Se_{10})_4]^{8-}$ supertetrahedron according to eq 2:

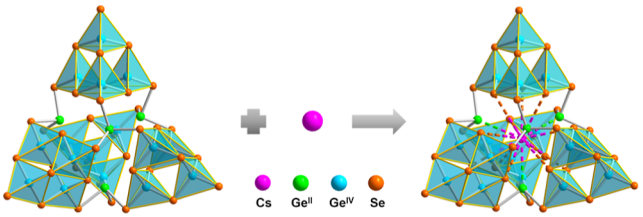

Figure 4. Illustration of the uptake of a Cs^+ ion by the surrounding $\{Ge_{20}Se_{40}\}^{8-}$ cage, according to eq 1. Notably, the calculated clusters symmetrize during geometry optimization.

$$E_B = E([A@Ge_4(Ge_4Se_{10})_4]^{7-}) - E(A^+) - E(Ge_4(Ge_4Se_{10})_4{}^{8-}) \quad (2)$$

We calculated bond energies E_B of −47.6 (Cs^+), −65.0 (Rb^+), −61.8 (K^+), −25.7 (Na^+), and −15.8 (Li^+) kJ/mol. The differences between the energies obtained for Cs^+, Rb^+, and K^+ are small, so the prediction of whether one of them is more stable than the others is beyond the accuracy of this model, but these numbers suggest that, in theory, K^+ and Rb^+ could also be accommodated in the cavity provided by the *pseudo*-P2 type cluster architecture. However, it is worth noting that all cations smaller than Cs^+ show an increasing tendency of adopting an unsymmetrical off-center position. Distances from the center of gravity are 0.0 (Cs^+), 0.1 (Rb^+), 37.2 (K^+), 147.4 (Na^+), and 219.4 (Li^+) pm. The cavity thus seems to be perfectly adopted to the needs of a symmetrical Cs^+ inclusion, as a valuable precondition for crystallization.

To experimentally explore the selectivity of compound **1** for Cs^+ cations, we designed and performed a comprehensive series of cross-experiments, as detailed in Scheme S1 and summarized in Table 1. All reaction conditions were the same as those for the preparation of compound **1** (see Scheme S1, left hand side), except for the use of other alkali metal salts of the $[Ge_4Se_{10}]^{4-}$ reactant, namely, $[Li_4(H_2O)_{20.33}][Ge_4Se_{10}]$, $Na_4[Ge_4Se_{10}]$, $[K_4(H_2O)_3][Ge_4Se_{10}]$, or $Rb_4[Ge_4Se_{10}]$, and the addition of binary salts of other alkali metal salts, CsCl, NaCl, KCl, RbCl, or NaCl + CsCl, to the original or modified reaction mixtures.

Reproducibly, the use of $[Li_4(H_2O)_{20.33}][Ge_4Se_{10}]$, $Na_4Ge_4Se_{10}$, $[K_4(H_2O)_3][Ge_4Se_{10}]$, or $Rb_4[Ge_4Se_{10}]$ did not afford crystals of compound **1** (see Scheme S1a) but led to the crystallization of crystals of compound $(C_2C_1Im)_6[Ge_8Se_{19}]$ that we reported recently.[20] As detailed in Scheme S1b, the addition of CsCl to such a reaction mixture caused the formation of compound **1** in all cases, as verified by SC-XRD. In addition, the yield of **1** from all controlled combinations is close to the number of the single-source formed one and is listed in Table S13.

As an example, we elaborate here on the result obtained for the mixture of $[K_4(H_2O)_3][Ge_4Se_{10}]$ with CsCl as the starting material: In the first refinement procedure, the Q peak on the difference Fourier map representing the embedded cation was assigned the atom form factor of a K atom (Figure S15a), which yielded inacceptable *R*1 and *wR*2 values of 0.1176 and 0.3277, respectively (Figure S15b). In the second refinement procedure, the inner Q peak was assigned the atom form factor of a Cs atom instead (Figure S15c), which led to a significant improvement of the final *R*1 and *wR*2 values of 0.0814 and 0.2248, respectively (Figure S15d). The result is in agreement with the fact that the difference Fourier map after refinement indicates a clear under-assignment of electron density around the embedded site if it is considered to be a K atom, whereas it is a perfect match when regarded as a Cs atom (see Figure S15a,c). The series of cross-experiments proved the high selectivity of the crystal structure of compound **1** for inclusion of Cs^+ as compared to that of the lighter congeners (Scheme S1c–f).

Furthermore, the preference for Cs^+ during the crystallization process was demonstrated by semiquantitative EDX of the as-synthesized crystals (see Figure S16). According to these data, Cs^+ is preferred for all combinations of reactants. In comparison with other alkali metals, the Cs content is predominant in compound **1**; however, we were able to detect trace amounts of Li^+, Na^+, K^+, or Rb^+. At first glance, the amount of the other alkali metals seems to increase in this order (as expected with regard to the ion radius approaching

https://doi.org/10.1021/jacs.2c13523
J. Am. Chem. Soc. 2023, 145, 3802−3811

Table 1. Summary of Experiments Undertaken to Explore the Selectivity of Compound 1 for Alkali Metal Ions[a]

	no additional ACl	CsCl	NaCl	KCl	RbCl	NaCl + CsCl
$[Li_4(H_2O)_{20.33}][Ge_4Se_{10}]$	×	√	×	×	×	√
$Na_4[Ge_4Se_{10}]$	×	√	×	×	×	√
$[K_4(H_2O)_3][Ge_4Se_{10}]$	×	√	×	×	×	√
$Rb_4[Ge_4Se_{10}]$	×	√	×	×	×	√
$[Cs_4(H_2O)][Ge_4Se_{10}]$	√	√	√	√	√	√

[a]√ denotes that we were able to crystallize compound 1; × denotes that we were not able to isolate compound 1

the one of Cs^+); however, the results need to be taken with a grain of salt as the errors of these measurements are very different and increase with smaller amounts.

On one hand, this result is in line with the DFT study as it suggests that it is generally possible to include K^+ or Rb^+. However, this inclusion is very minor only, supporting the assumption that the distortion, which is only observed in the crystal structure (while the assembly relaxes into a higher symmetry during geometry optimization by quantum chemistry), causes the high selectivity for Cs^+ owing to a thus perfect match of the ionic radius of the inner ion with the cavity. In addition, this underscores the meaningfulness of actually crystallizing the compound for ion separation.

A final proof for the inclusion of Cs^+ in the cluster anion of isolated compound **1** was obtained by means of ESI-MS, as a powerful tool for the investigation of precise compositions. Isolated and washed single crystals obtained from the ionothermal reaction of $[K_4(H_2O)_3][Ge_4Se_{10}]$ with CsCl were dissolved in DMF, and the fresh solutions were investigated. We were able to detect a series of signals of the $[Cs@Ge^{II}_4(Ge^{IV}_4Se_{10})_4]^{q-}$ anion along with different numbers of counterions or H^+ and thus with charges ranging from 4− to 3− and 2− (Figure S17). The experimental isotope patterns show perfect agreement with the simulated ones. The dominant signals can be assigned to species of the formulas $\{(C_6N_2H_{11})_{3-x}H_xCs@Ge_4(Ge_4Se_{10})_4\}^{4-}$ (x = 0−2; Figure S18). An overlap with the isotope pattern of $\{(C_6N_2H_{11})_{3-x}H_xK@Ge_4(Ge_4Se_{10})_4\}^{4-}$ is coincidently caused by the similar molecular weight of the $(C_2C_1Im)^+$ cation and the difference between the atomic weights of Cs and K. As indicated in detail for the high-resolution mass peaks of $\{(C_6N_2H_{11})_2H_1Cs@Ge_4(Ge_4Se_{10})_4\}^{4-}$ and $\{(C_6N_2H_{11})_3K@Ge_4(Ge_4Se_{10})_4\}^{4-}$ (see Figure S18a), the isotope patterns exhibit very similar m/z values, but that of $\{(C_6N_2H_{11})_3K@Ge_4(Ge_4Se_{10})_4\}^{4-}$ shows completely different relative abundances as compared to the experimental spectrum. In order to further distinguish the compositions, the mass spectra of the cluster anion with 3^- charge, which amplifies the difference between simulated and experimental patterns due to the lower charge, are provided in Figure 5.

Clearly, the simulated mass peaks of the species $\{(C_6N_2H_{11})_{3-x}H_xK@Ge_4(Ge_4Se_{10})_4\}^{3-}$ (Figure 5b) differ from those appearing in the experimental spectrum, whereas the mass peaks of $\{(C_6N_2H_{11})_{4-x}H_xCs@Ge_4(Ge_4Se_{10})_4\}^{3-}$ (Figure 5a) are an excellent match with the experimental ones (for more details, see Figures S18—S21). The mass spectra thus demonstrate both the integrity of the supramolecular cluster assembly (along with counterions) in solution and in the gas phase and the formation of $[Cs@Ge_4(Ge_4Se_{10})_4]^{7-}$ instead of $[K@Ge_4(Ge_4Se_{10})]^{7-}$ during crystallization.

Another series of experiments were undertaken to investigate the selective incorporation of Na^+ during

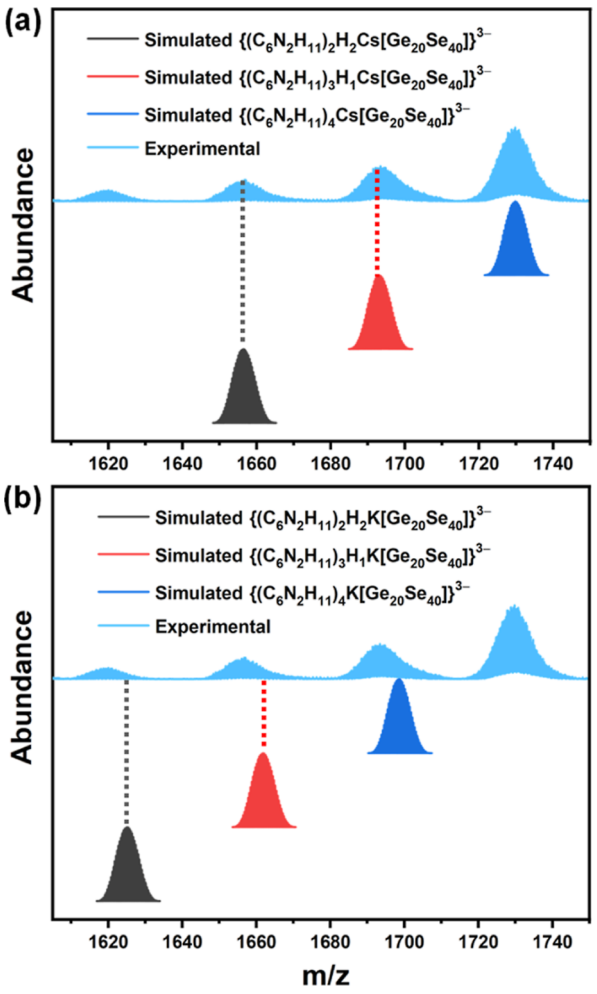

Figure 5. Comparison of mass peaks of the experimental ESI-MS spectrum with (a) simulated mass spectra of $\{(C_6N_2H_{11})_2H_2Cs@Ge_4(Ge_4Se_{10})_4\}^{3-}$, $\{(C_6N_2H_{11})_3H_1Cs@Ge_4(Ge_4Se_{10})_4\}^{3-}$, and $\{(C_6N_2H_{11})_4Cs@Ge_4(Ge_4Se_{10})_4\}^{3-}$ (black, red, and blue, respectively) and with (b) simulated mass spectra of $\{(C_6N_2H_{11})_2H_2K@Ge_4(Ge_4Se_{10})_4\}^{3-}$, $\{(C_6N_2H_{11})_3H_1K@Ge_4(Ge_4Se_{10})_4\}^{3-}$, and $\{(C_6N_2H_{11})_4K@Ge_4(Ge_4Se_{10})_4\}^{3-}$ (black, red, and blue, respectively), indicating the perfect fit if the presence of Cs^+ is assumed (a) and the misfit if the presence of K^+ is assumed (b).

crystallization of compound **2a**, which are summarized in Table 2 and Scheme S2. We restricted the study to a cross-check of the most closely related K^+ as the competing ion during the crystallization process as this already ruled out the necessity to continue with the less similar ones. When the reaction conditions were the same as those for the formation of compound **2a** (see Scheme S2), yet with the replacement of $[Na_4(H_2O)_{14}][GeSe_4]$ with $[K_4(H_2O)_4][GeSe_4]$, we failed to crystallize a similar crystal structure with K^+ embedded inside

https://doi.org/10.1021/jacs.2c13523
J. Am. Chem. Soc. 2023, 145, 3802−3811

Table 2. Summary of Experiments Undertaken to Explore the Selectivity of Compound 2a for Alkali Metal Ions[a]

	no additional ACl	NaCl
$[Na_4(H_2O)_{14}][GeSe_4]$	√	√
$[K_4(H_2O)_4][GeSe_4]$	×	√

[a]√ denotes that we were able to crystallize compound 2a; × denotes that we were not able to isolate target compound 2a

the heterometallic supramolecular cage (Table 2). However, crystals could be isolated upon the addition of NaCl and $[K_4(H_2O)_4][GeSe_4]$, which was confirmed by means of SC-XRD measurements and refinement. According to the difference Fourier maps, all the embedded A^+ atoms were determined to be exclusively Na^+. As expected, *R*1 and *wR*2 values do not differ a lot but still indicate a preference for the assignment of Na to the site of the A atom (0.0502 and 0.1243, respectively; Figure S22a,b) as compared to the assignment of K to this site (0.0545 and 0.1345, respectively; Figure S22c,d). These results are supported by EDX measurements (see Figure S23). The polymeric nature of the anionic substructure inhibits the compounds' solubility; hence, mass spectrometric analyses could not be performed. The same holds for molecular quantum chemistry. However, the experimental proofs given above are all aligned and clearly indicate that compounds **2a** and **2b** are based exclusively on the ion-selective cluster assembly with the aid of Na^+ and Cu^+.

4. CONCLUSIONS

By crystallization from ionothermal reactions, we were able to introduce the ion-selective assembly of supertetrahedral clusters into discrete or polyhedral supramolecular assemblies based on $[Ge_4Se_{10}]^{4-}$ anions. The discrete substructure, which represents a defect- or *pseudo*-P2-type architecture, is the largest supertetrahedral selenido germanate anion and the first one to feature Ge^{II} and Ge^{IV} coexisting in supertetrahedral chalcogenides. The polymeric substructures, which were isolated in two crystalline polymorphs, form two dimensional layers that are based on similar supramolecular cluster assemblies but differ in detail owing to the additional incorporation of Cu^+. Both types of compounds exhibit an exclusive selectivity for one type of alkali metal cations included in the crystalline compound, Cs^+ in the case of the discrete clusters and Na^+ for the triheterometallic cluster polymer, as indicated by a variety of analytical methods. We suggest such compounds as models for further ion-selective cluster assemblies in crystalline phases, as a useful tool for targeted ion capture and separation.

■ ASSOCIATED CONTENT

Supporting Information

The Supporting Information is available free of charge at https://pubs.acs.org/doi/10.1021/jacs.2c13523.

Additional details on crystal photographs, X-ray diffraction analyses, EDX measurements, XPS, and ESI-MS analyses (PDF)

CIFs of compounds **1**, **2a**, and **2b** (TXT)

Accession Codes

CCDC 2178545−2178547 contain the supplementary crystallographic data for this paper. These data can be obtained free of charge via www.ccdc.cam.ac.uk/data_request/cif, or by emailing data_request@ccdc.cam.ac.uk, or by contacting The Cambridge Crystallographic Data Centre, 12 Union Road, Cambridge CB2 1EZ, UK; fax: +44 1223 336033.

■ AUTHOR INFORMATION

Corresponding Author

Stefanie Dehnen − *Institute of Nanotechnology (INT) and Karlsruhe Nano Micro Facility (KNMF), Karlsruhe Institute of Technology (KIT), 76344 Eggenstein-Leopoldshafen, Germany*; orcid.org/0000-0002-1325-9228; Email: stefanie.dehnen@kit.edu

Authors

Zhou Wu − *Institute of Nanotechnology (INT) and Karlsruhe Nano Micro Facility (KNMF), Karlsruhe Institute of Technology (KIT), 76344 Eggenstein-Leopoldshafen, Germany*

Florian Weigend − *Fachbereich Chemie and Wissenschaftliches Zentrum für Materialwissenschaften, Philipps-Universität Marburg, 35043 Marburg, Germany*; orcid.org/0000-0001-5060-1689

Dieter Fenske − *Institute of Nanotechnology (INT) and Karlsruhe Nano Micro Facility (KNMF), Karlsruhe Institute of Technology (KIT), 76344 Eggenstein-Leopoldshafen, Germany*

Tim Naumann − *Fachbereich Chemie and Wissenschaftliches Zentrum für Materialwissenschaften, Philipps-Universität Marburg, 35043 Marburg, Germany*

J. Michael Gottfried − *Fachbereich Chemie and Wissenschaftliches Zentrum für Materialwissenschaften, Philipps-Universität Marburg, 35043 Marburg, Germany*; orcid.org/0000-0001-5579-2568

Complete contact information is available at: https://pubs.acs.org/10.1021/jacs.2c13523

Author Contributions

The manuscript was written through contributions of all authors.

Notes

The authors declare no competing financial interest.

■ ACKNOWLEDGMENTS

This work was financially supported by the German Research Foundation (Deutsche Forschungsgemeinschaft, DFG). Z.W. acknowledges a PhD fellowship by the China Scholarship Council (CSC no. 202006920030). We thank Prof. Dr. J. Janek and Dr. J. Sann for fruitful discussion and their help regarding XPS analyses.

■ ABBREVIATIONS

A^+	alkali metal ions
SC-XRD	single-crystal X-ray diffraction
EDX	energy-dispersive X-ray spectroscopy
XPS	X-ray photoelectron spectroscopy
ESI-MS	electrospray ionization mass spectroscopy.

■ REFERENCES

(1) Lu, J.; Zhang, H.; Hou, J.; Li, X.; Hu, X.; Hu, Y.; Easton, C. D.; Li, Q.; Sun, C.; Thornton, A. W.; Hill, M. R.; Zhang, X.; Jiang, G.; Liu, J. Z.; Hill, A. J.; Freeman, B. D.; Jiang, L.; Wang, H. Efficient Metal Ion Sieving in Rectifying Subnanochannels Enabled by Metal−Organic Frameworks. *Nat. Mater.* **2020**, *19*, 767−774.

(2) Zhang, H.; Hou, J.; Hu, Y.; Wang, P.; Ou, R.; Jiang, L.; Liu, Z.; Freeman, D.; Hill, J.; Wang, H. Ultrafast Selective Transport of Alkali

Metal Ions in Metal Organic Frameworks with Subnanometer Pores. *Sci. Adv.* **2018**, *4*, No. eaaq0066.
(3) Bögels, G. M.; Lugger, J. A. M.; Goor, O. J. G. M.; Sijbesma, R. P. Size-selective Binding of Sodium and Potassium Ions in Nanoporous Thin Films of Polymerized Liquid Crystals. *Adv. Funct. Mater.* **2016**, *26*, 8023−8030.
(4) Ma, W.; Lv, T.-T.; Tang, J.-H.; Feng, M.-L.; Huang, X.-Y. Highly Efficient Uptake of Cs^+ by Robust Layered Metal−Organic Frameworks with a Distinctive Ion Exchange Mechanism. *JACS Au* **2022**, *2*, 492−501.
(5) Han, E.; Kim, Y.-G.; Yang, H.-M.; Yoon, I.-H.; Choi, M. Synergy between Zeolite Framework and Encapsulated Sulfur for Enhanced Ion-exchange Selectivity to Radioactive Cesium. *Chem. Mater.* **2018**, *30*, 5777−5785.
(6) Hanada, T.; Goto, M. Synergistic Deep Eutectic Solvents for Lithium Extraction. *ACS Sustain. Chem. Eng.* **2021**, *9*, 2152−2160.
(7) He, Q.; Williams, N. J.; Oh, J. H.; Lynch, V. M.; Kim, S. K.; Moyer, B. A.; Sessler, J. L. Selective Solid−Liquid and Liquid−Liquid Extraction of Lithium Chloride Using Strapped Calix[4]pyrroles. *Angew. Chem., Int. Ed.* **2018**, *57*, 11924−11928.
(8) Gohil, H.; Chatterjee, S.; Yadav, S.; Suresh, E.; Paital, A. R. An Ionophore for High Lithium Loading and Selective Capture from Brine. *Inorg. Chem.* **2019**, *58*, 7209−7219.
(9) He, Q.; Zhang, Z.; Brewster, J. T.; Lynch, V. M.; Kim, S. K.; Sessler, J. L. Hemispherand-strapped Calix[4]pyrrole: An Ion-pair Receptor for the Recognition and Extraction of Lithium Nitrite. *J. Am. Chem. Soc.* **2016**, *138*, 9779−9782.
(10) Razmjou, A.; Asadnia, M.; Hosseini, E.; Habibnejad Korayem, A.; Chen, V. Design Principles of Ion Selective Nanostructured Membranes for the Extraction of Lithium Ions. *Nat. Commun.* **2019**, *10*, 5793.
(11) Guo, Y.; Ying, Y.; Mao, Y.; Peng, X.; Chen, B. Polystyrene Sulfonate Threaded through a Metal−Organic Framework Membrane for Fast and Selective Lithium-ion Separation. *Angew. Chem., Int. Ed.* **2016**, *55*, 15120−15124.
(12) Ye, T.; Hou, G.; Li, W.; Wang, C.; Yi, K.; Liu, N.; Liu, J.; Huang, S.; Gao, J. Artificial Sodium-selective Ionic Device based on Crown-ether Crystals with Subnanometer Pores. *Nat. Commun.* **2021**, *12*, 5231.
(13) Celestian, A. J.; Kubicki, J. D.; Hanson, J.; Clearfield, A.; Parise, J. B. The Mechanism Responsible for Extraordinary Cs Ion Selectivity in Crystalline Silicotitanate. *J. Am. Chem. Soc.* **2008**, *130*, 11689−11694.
(14) Zhang, B.; Sun, H.-Y.; Li, J.; Li, L.-Z.; Deng, Y.-L.; Liu, S.-H.; Feng, M.-L.; Huang, X.-Y. Fast and Selective Removal of Aqueous Uranium by a K^+-activated Robust Zeolitic Sulfide with Wide pH Resistance. *Inorg. Chem.* **2019**, *58*, 11622−11629.
(15) Yang, H.; Luo, M.; Luo, L.; Wang, H.; Hu, D.; Lin, J.; Wang, X.; Wang, Y.; Wang, S.; Bu, X.; Feng, P.; Wu, T. Highly Selective and Rapid Uptake of Radionuclide Cesium Based on Robust Zeolitic Chalcogenide via Stepwise Ion-exchange Strategy. *Chem. Mater.* **2016**, *28*, 8774−8780.
(16) Li, W.-A.; Peng, Y.-C.; Ma, W.; Huang, X.-Y.; Feng, M.-L. Rapid and Selective Removal of Cs^+ and Sr^{2+} Ions by Two Zeolite-type Sulfides via Ion Exchange Method. *Chem. Eng. J.* **2022**, *442*, 136377.
(17) Zhang, X.-M.; Sarma, D.; Wu, Y.-Q.; Wang, L.; Ning, Z.-X.; Zhang, F.-Q.; Kanatzidis, M. G. Open-framework Oxysulfide Based on the Supertetrahedral $[In_4Sn_{16}O_{10}S_{34}]^{12-}$ Cluster and Efficient Sequestration of Heavy Metals. *J. Am. Chem. Soc.* **2016**, *138*, 5543−5546.
(18) Zeng, X.; Liu, Y.; Zhang, T.; Jin, J.-C.; Li, J.-L.; Sun, Q.; Ai, Y.-J.; Feng, M.-L.; Huang, X.-Y. Ultrafast and Selective Uptake of Eu^{3+} from Aqueous Solutions by Two Layered Sulfides. *Chem. Eng. J.* **2021**, *420*, 127613.
(19) Xiao, C.; Hassanzadeh Fard, Z.; Sarma, D.; Song, T.-B.; Xu, C.; Kanatzidis, M. G. Highly Efficient Separation of Trivalent Minor Actinides by a Layered Metal Sulfide ($KInSn_2S_6$) from Acidic Radioactive Waste. *J. Am. Chem. Soc.* **2017**, *139*, 16494−16497.
(20) Wu, Z.; Nußbruch, I.; Nier, S. S.; Dehnen, S. Ionothermal Access to Defined Oligomers of Supertetrahedral Selenido Germanate Clusters. *JACS Au* **2022**, *2*, 204−213.
(21) Zhang, J.; Feng, P.; Bu, X.; Wu, T. Atomically Precise Metal Chalcogenide Supertetrahedral Clusters: Frameworks to Molecules, and Structure to Function. *National Science Review* **2022**, *9*, nwab076.
(22) Zhang, J.; Bu, X.; Feng, P.; Wu, T. Metal Chalcogenide Supertetrahedral Clusters: Synthetic Control over Assembly, Dispersibility, and Their Functional Applications. *Acc. Chem. Res.* **2020**, *53*, 2261−2272.
(23) Liu, Y.; Zhang, J.; Han, B.; Wang, X.; Wang, Z.; Xue, C.; Bian, G.; Hu, D.; Zhou, R.; Li, D.-S.; Wang, Z.; Ouyang, Z.; Li, M.; Wu, T. New Insights into Mn−Mn Coupling Interaction-directed Photoluminescence Quenching Mechanism in Mn^{2+}-doped Semiconductors. *J. Am. Chem. Soc.* **2020**, *142*, 6649−6660.
(24) Peters, B.; Lichtenberger, N.; Dornsiepen, E.; Dehnen, S. Current Advances in Tin Cluster Chemistry. *Chem. Sci.* **2020**, *11*, 16−26.
(25) Lv, J.; Zhang, J.; Xue, C.; Hu, D.; Wang, X.; Li, D.-S.; Wu, T. Two Penta-supertetrahedral Cluster-based Chalcogenide Open Frameworks: Effect of the Cluster Spatial Connectivity on the Electron-transport Efficiency. *Inorg. Chem.* **2019**, *58*, 3582−3585.
(26) Wu, Z.; Wang, X.-L.; Hu, D.; Wu, S.; Liu, C.; Wang, X.; Zhou, R.; Li, D.-S.; Wu, T. A New Cluster-based Chalcogenide Zeolite Analogue with A Large Inter-cluster Bridging Angle. *Inorg. Chem. Front.* **2019**, *6*, 3063−3069.
(27) Xu, X.; Wang, W.; Liu, D.; Hu, D.; Wu, T.; Bu, X.; Feng, P. Pushing up the Size Limit of Metal Chalcogenide Supertetrahedral Nanocluster. *J. Am. Chem. Soc.* **2018**, *140*, 888−891.
(28) Peng, Y.; Hu, Q.; Liu, Y.; Li, J.; Huang, X. Discrete Supertetrahedral Tn Chalcogenido Clusters Synthesized in Ionic Liquids: Crystal Structures and Photocatalytic Activity. *ChemPlusChem* **2020**, *85*, 2487−2498.
(29) Lin, Q.; Bu, X.; Feng, P. An Infinite Square Lattice of Super-supertetrahedral T6-like Tin Oxyselenide Clusters. *Chem. Commun.* **2014**, *50*, 4044−4046.
(30) Santner, S.; Wolff, A.; Ruck, M.; Dehnen, S. Multi-valent Group 14 Chalcogenide Architectures from Ionic Liquids: 0D-$\{[Cs@Sn^{II}_4(Ge^{IV}_4Se^{10})_4]^{7-}\}$ and 2D-$\{[Sn^{II}(Ge^{IV}_4Se_{10})]^{2-}$. *Chem. Eur. J.* **2018**, *24*, 11899−11903.
(31) Krebs, B.; Jacobsen, H. J. Darstellung und Struktur von $Na_4GeSe_4{\cdot}14H_2O$. *Z. Anorg. Allg. Chem.* **1976**, *421*, 97−104.
(32) Duchardt, M.; Haddadpour, S.; Kaib, T.; Bron, P.; Roling, B.; Dehnen, S. Different Chemical Environments of $[Ge_4Se_{10}]^{4-}$ in the Li^+ Compounds $[Li_4(H_2O)_{16}][Ge_4Se_{10}]{\cdot}4.33H_2O$, $[\{Li_4(thf)_{12}\}Ge_4Se_{10}]$, and $[Li_2(H_2O)_8][MnGe_4Se_{10}]$, and Ionic Conductivity of Underlying "$Li_4Ge_4Se_{10}$". *Inorg. Chem.* **2021**, *60*, 5224−5231.
(33) Eisenmann, B.; Hansa, J. Crystal structure of tetrasodium decaselenotetragermanate, $Na_4[Ge_4Se_{10}]$. *Z Krist-Cryst Mater.* **1993**, *205*, 325−326.
(34) Wachhold, M.; Kanatzidis, M. G. Surfactant-Templated Inorganic Lamellar and Non-lamellar Hybrid Phases Containing Adamantane $[Ge_4Se_{10}]^{4-}$ Anions. *Chem. Mater.* **2000**, *12*, 2914−2923.
(35) Melullis, M.; Dehnen, S. S. Crystal Structures, UV-Vis Spectra and First NMR Spectra of New Potassium Salts of Chalcogenogermanates. *Z. Anorg. Allg. Chem.* **2007**, *633*, 2159−2167.
(36) Klepp, K. O.; Fabian, F. New Chalcogenogermanates with Adamantane Type Complex Anions: Preparation and Crystal Structures of $K_4Ge_4S_{10}$; $Rb_4Ge_4S_{10}$, $Rb_4Ge_4Se_{10}$, and $Cs_4Ge_4Se_{10}$. *Z. Naturforsch. B* **1999**, *54*, 1499−1504.
(37) Sheldrick, G. SHELXT - Integrated Space-group and Crystal-structure Determination. *Acta Cryst* **2015**, *71*, 3−8.
(38) Sheldrick, G. Crystal Structure Refinement with SHELXL. *Acta Cryst* **2015**, *71*, 3−8.
(39) Spek, A. Structure Validation in Chemical Crystallography. *Acta Cryst* **2009**, *65*, 148−155.
(40) van der Sluis, P.; Spek, A. L. BYPASS: an Effective Method for the Refinement of Crystal Structures Containing Disordered Solvent Regions. *Acta Cryst* **1990**, *46*, 194−201.

https://doi.org/10.1021/jacs.2c13523
J. Am. Chem. Soc. 2023, 145, 3802−3811

(41) Diamond - Crystal and Molecular Structure Visualization, Crystal Impact in Putz, Dr. H.; Brandenburg, Dr. K., Eds. *GbR: Kreuzherrenstr. 102*, 53227 Bonn, Germany, http://www.crystalimpact.com/diamond 2023 (accessed 01 05, 2023)
(42) Turbomole, Version 7.6 2021, a development of University of Karlsruhe and Forschungszentrum Karlsruhe GmbH 1989−2007, TURBOMOLE GmbH since 2007, available via https://www.turbomole.org 2007 (accessed 01 05, 2023).
(43) Perdew, J. P.; Burke, K.; Ernzerhof, M. Generalized Gradient Approximation Made Simple. *Phys. Rev. Lett.* **1996**, *77*, 3865−3868.
(44) Peng, D.; Middendorf, N.; Weigend, F.; Reiher, M. An efficient implementation of two-component relativistic exact-decoupling methods for large molecules. *J. Chem. Phys.* **2013**, *138*, 184105.
(45) Franzke, Y. J.; Middendorf, N.; Weigend, F. Efficient implementation of one- and two-component analytical energy gradients in exact two-component theory. *J. Chem. Phys.* **2018**, *148*, 104110.
(46) Pollak, P.; Weigend, F. Segmented Contracted Error-Consistent Basis Sets of Double- and Triple-ζ Valence Quality for One- and Two-Component Relativistic All-Electron Calculations. *J. Chem. Theory Comput.* **2017**, *13*, 3696.
(47) Schäfer, A.; Klamt, A.; Sattel, D.; Lohrenz, J. C. W.; Eckert, F. COSMO Implementation in TURBOMOLE: Extension of an efficient quantum chemical code towards liquid systems. *Phys. Chem. Chem. Phys.* **2000**, *2*, 2187.
(48) Zhang, J.; Qin, C.; Zhong, Y.; Wang, X.; Wang, W.; Hu, D.; Liu, X.; Xue, C.; Zhou, R.; Shen, L.; Song, Y.; Xu, D.; Lin, Z.; Guo, J.; Su, H.; Li, D.-S.; Wu, T. Atomically Precise Metal-chalcogenide Semiconductor Molecular Nanoclusters with High Dispersibility: Designed Synthesis and Intracluster Photocarrier Dynamics. *Nano Res.* **2020**, *13*, 2828−2836.
(49) Zheng, N.; Bu, X.; Feng, P. Pentasupertetrahedral Clusters as Building Blocks for a Three-Dimensional Sulfide Superlattice. *Angew. Chem., Int. Ed.* **2004**, *43*, 4753−4755.
(50) Eichhöfer, A.; Fenske, D. Syntheses and Structures of New Copper(I)−indium(III)−selenide Clusters. *J. Chem. Soc., Dalton Trans.* **2000**, 941−944.
(51) Zheng, N.; Bu, X.; Wang, B.; Feng, P. Microporous and Photoluminescent Chalcogenide Zeolite Analogs. *Science* **2002**, *298*, 2366−2369.

https://doi.org/10.1021/jacs.2c13523
J. Am. Chem. Soc. 2023, 145, 3802−3811